American Mineralogist, Volume 94, pages 74–82, 2009

Structural features in Tutton's salts $K_2[M^{2+}(H_2O)_6](SO_4)_2$, with M^{2+} = Mg, Fe, Co, Ni, Cu, and Zn

FERDINANDO BOSI,[1,2,*] GIROLAMO BELARDI,[3] AND PAOLO BALLIRANO[1,3]

[1]Dipartimento di Scienze della Terra, Università di Roma "La Sapienza," Piazzale Aldo.Moro 5, 00185 Roma, Italy
[2]Department of Mineralogy, Swedish Museum of Natural History, Box 50007, 10405 Stockholm, Sweden
[3]CNR-IGAG Istituto di Geologia Ambientale e Geoingegneria, Sede di Roma, Via Bolognola 7, 00138 Roma, Italy

ABSTRACT

The crystal chemistry of six crystals of general formula $K_2[M^{2+}(H_2O)_6](SO_4)_2$, with M^{2+} = Mg, Fe, Co, Ni, Cu, and Zn, was investigated by single-crystal structure analysis to determine the effects of the chemical variation of M^{2+} on the structural environment surrounding K, *M*, and S sites. Results indicate that the distortion in the SO_4 tetrahedron and the MO_6 octahedron is very small, except for CuO_6 where it is pronounced because of the Jahn-Teller effect. The KO_8-octacoordinate polyhedron has the highest degree of distortion, and its idealized shape may be referred to as a bicapped trigonal prism. The SO_4 size is not affected by changes in cation occupancies at the adjacent *M* site. In contrast, changes in the KO_8 size, which are accompanied by changes in the bond valence sum at K, depend on interaction with the first and second coordination sphere of *M*. This interaction results by changes in *M*-O individual lengths, by expansion of the second coordination sphere of *M*, and by changes in the distribution of the bond strengths over the O atoms coordinated to K. The MO_6 size follows the expected trend from the increased ionic radius at the *M* site. The latter is also correlated with the unit-cell volume except for the Cu- and Mg-phase, which show a larger cell volume with respect to that expected. Although the relevant octahedral distortion around the Cu^{2+} cation explains the volume excess in the Cu-phase, an expansion of the second coordination sphere of Mg^{2+}, compared to those of cations of larger ionic radius (such as Zn and Co), explains the excess of the unit-cell volume in the Mg-phase. As the CuO_6 distortion can be caused by the Jahn-Teller effect, the higher ionicity of the Mg atom could be the cause for its anomalous behavior observed in Tutton's salts. This stereochemical behavior of the Mg atom seems to be consistent with the weakening of the hydrogen bonds in the structure connected to differences in the bonding character of Mg and transition metals when coordinated by water molecules.

Keywords: Crystal synthesis, Tutton's salts, crystal structure, bond valence

INTRODUCTION

Tutton's salts are a group of compounds described by the general formula $A_2[M^{2+}(H_2O)_6](XO_4)_2$, where *A* is an univalent cation (K^+, Cs^+, Rb^+, Tl^+, etc.) or NH_4^+, M^{2+} a divalent cation such as Mg^{2+}, V^{2+}, Cr^{2+}, Mn^{2+}, Fe^{2+}, Co^{2+}, Ni^{2+}, Cu^{2+}, Zn^{2+}, Cd^{2+}, and $X = S^{6+}$ or Se^{6+}. All compounds crystallize in the monoclinic system, space group $P2_1/a$. Compounds with NH_4 (Cotton et al. 1993), Rb (Euler et al. 2000), and Cs (Euler et al. 2003) have been systematically characterized and, especially for the ammonium compounds, a large number of structural data are available. In contrast, the crystal chemistry of the K-containing series has not been systematically investigated yet and in the case of $K_2[Mg(H_2O)_6](SO_4)_2$, the single-crystal structural data (Kannan and Viswamitra 1965) are not of adequate quality.

In nature, only a limited number of minerals corresponding to the formula $A_2[M^{2+}(H_2O)_6](SO_4)_2$ have been found and, according to the Strunz classification, they are grouped under the picromerite group: picromerite $K_2[Mg(H_2O)_6](SO_4)_2$, cyanochroite $K_2[Cu(H_2O)_6](SO_4)_2$, boussingaultite $(NH_4)_2[Mg(H_2O)_6](SO_4)_2$, nickel-boussingaultite $(NH_4)_2[Ni(H_2O)_6](SO_4)_2$, and mohrite $(NH_4)_2[Fe(H_2O)_6](SO_4)_2$. These sulfate minerals are typically found as products of fumaroles and geysers (Larsen and Shannon 1920; Garavelli 1964), on underground ore stockpiles (Yakhontova et al. 1976), tailings impoundments (Agnew 1998), in evaporite deposits (Spencer 2000), and they have also been proposed to be present on Europa's surface (Zoltov and Shock 2001). In particular, evaporite deposits preserve a wealth of information on Earth's past surface conditions and, in this context, sulfate minerals are geologically important phases in understanding the hydrochemistry of ancient surface waters (Spencer 2000). Picromerite is a phase involved in alkaline brine systems low in Ca (Spencer 2000) and in the model regarding the bulk primordial hydrosphere on Mars (King et al. 2004). In recent years, picromerite has received interest in material sciences for its optical applications (e.g., Dhandapani et al. 2006).

The aim of this paper is to carry out a crystal-chemical study of the synthetic compounds of general formula $K_2[M^{2+}(H_2O)_6](SO_4)_2$, with M^{2+} = Mg, Fe, Co, Ni, Cu, and Zn (acronyms: KMgS, KFeS, KCoS, KNiS, KCuS, and KZnS, respectively). As the Tutton's salts represent a remarkable example of isotypic structures extending right across the first transition series cations, they

* E-mail: ferdinando.bosi@uniroma1.it

provide the opportunity to determine the effects of the chemical variation of M^{2+} on the structural environment surrounding K, *M*, and S sites, and on unit-cell parameters.

Experimental methods

Synthesis

Crystals of Tutton's salts were prepared by dissolving K_2SO_4 (Merck P.A.) and $MSO_4{\cdot}nH_2O$ salts p.a. in double deionized water with a variable salt molar fraction, defined as $K_2SO_4/(K_2SO_4 + MSO_4)$, (Table 1). Solutions were kept at a pH of about 6.2, except for the case of the crystallization of KFeS, and the solvent was subsequently allowed to slowly evaporate at a temperature within the stability field of the relevant compound. The salt fraction and the temperature of crystallization were obtained for each Tutton's salt from TX-phase stability diagrams calculated using the Extended UNIQUAC Model (Thomsen et al. 1996). Stability fields were obtained for $K_2[M^{2+}(H_2O)_6](SO_4)_2$, with M^{2+} = Mg, Fe, Co, Ni, and Zn. The resulting crystals, in equilibrium with the mother solution, were removed and dried at room temperature. For Mn^{2+} and Cu^{2+}, calculations indicated that crystallization would have been obtained for non-equilibrium conditions only. However, only in the case of KCuS was the crystallization successful.

Single-crystal structural refinement

After preliminary optical examination, crystal fragments were selected for X-ray data collection with a four-circle Siemens *P*4 automated diffractometer. Unit-cell parameters were measured by centering 58 reflections in the range 8–45 °2θ. X-ray data were collected in the 3–70 °2θ range with the ω-scan method. Scan speed was variable, depending on reflection intensity, and was estimated with a pre-scan. The background was measured with a stationary crystal and counter at the beginning and the end of each scan, in both cases for half the scan time. All crystals were stable during measurement, except for KFeS; this crystal fairly quickly dehydrates to $K_2Fe(SO_4)_2{\cdot}4H_2O$ at room temperature (Ballirano and Belardi 2006).

Data reduction was performed with the SHELXTL-PC program package. Intensities were corrected for polarization and Lorentz effects. Absorption correction was accomplished with a semi-empirical method (North et al. 1968). Structural refinements were carried out with SHELXL-97 (Sheldrick 1997). Starting coordinates were taken from Simmons et al. (2006) for cyanochroite. The variable parameters were scale factor, extinction coefficient, fractional coordinates, and anisotropic displacement parameters (hydrogen atoms treated isotropically). Neutral scattering factors were used, except for oxygen and M^{2+} cations (half and fully ionized scattering factors, respectively, taken from the *International Tables for Crystallography*, vol. C, Wilson 1995), because they led to the best values of conventional agreement factors over all sinθ/λ intervals. No significant correlation between parameters was observed.

Experimental details and cell parameters are reported in Table 2, fractional coordinates and isotropic displacement parameters in Table 3, anisotropic displacement parameters in Table 4[1], relevant bond lengths and angles in Table 5, and bond valence analysis following Brese and O'Keeffe (1991) in Table 6.

Results and discussion

Geometrical features: Polyhedral distortions

The structure of Tutton's salts consists of $M^{2+}(H_2O)_6$ groups (=MO_6) linked to four KO_8 polyhedra via the equatorial oxygen atom belonging to water molecules, and to eight SO_4 sulfate by medium-strength hydrogen bonds (Fig. 1). Thus, a three-dimensional structure is formed by the S^{6+}, M^{2+}, and K^+ cations

[1] Deposit item AM-09-003, Table 4 (anisotropic displacement parameters). Deposit items are available two ways: For a paper copy contact the Business Office of the Mineralogical Society of America (see inside front cover of recent issue) for price information. For an electronic copy visit the MSA web site at http://www.minsocam.org, go to the American Mineralogist Contents, find the table of contents for the specific volume/issue wanted, and then click on the deposit link there.

Table 1. Details of the synthesis procedure of the analyzed Tutton's salts

Tutton's salt	Salts used P.A.	Salt fraction	pH of the solution	Crystallization *T* (°C)	Color of crystals
$K_2[Mg(H_2O)_6](SO_4)_2$	$K_2SO_4 + MgSO_4{\cdot}7H_2O$ Carlo Erba	0.22	6.2	31–35	cerulean white
$K_2[Fe(H_2O)_6](SO_4)_2$	$K_2SO_4 + FeSO_4{\cdot}7H_2O$ Riedel-De Haën AG	0.3	2.05 with H_2SO_4	21	fine pale-green unstable in air; quickly dehydrates to mereiterite
$K_2[Co(H_2O)_6](SO_4)_2$	$K_2SO_4 + CoSO_4{\cdot}7H_2O$ Riedel-De Haën AG	0.4	6.2	50	cyan
$K_2[Ni(H_2O)_6](SO_4)_2$	$K_2SO_4 + NiSO_4{\cdot}6H_2O$ Riedel-De Haën AG	0.5	6.2	65	brownish red
$K_2[Cu(H_2O)_6](SO_4)_2$	$K_2SO_4 + CuSO_4{\cdot}nH_2O$ Carlo Erba	0.5	6.2	21	metastable form—pale green
$K_2[Zn(H_2O)_6](SO_4)_2$	$K_2SO_4 + ZnSO_4{\cdot}7H_2O$ Riedel-De Haën AG	0.4	6.2	65	cerulean white

Table 2. Miscellaneous data of the structural refinement of Tutton's salts

	KMgS	KFeS	KCoS	KNiS	KCuS	KZnS
Space group			$P2_1/a$			
a (Å)	9.0954(3)	9.0822(4)	9.0609(4)	9.0049(4)	9.0851(4)	9.0449(6)
b (Å)	12.2484(5)	12.2786(7)	12.2156(6)	12.1904(8)	12.1302(6)	12.2213(10)
c (Å)	6.1335(3)	6.1765(4)	6.1586(4)	6.1368(5)	6.1674(4)	6.1592(6)
β (°)	104.880(3)	104.568(4)	104.839(4)	105.047(5)	104.450(4)	104.775(6)
V (Å^3)	660.38(5)	666.64(7)	658.93(6)	650.56(8)	658.17(6)	658.33(10)
Z			2			
Temperature (K)			293			
Wavelength			Mo*K*α (30 mA × 50kV)			
μ (cm^{-1})	11.483	21.360	23.179	25.198	26.760	28.820
Scan mode			ω			
Scan speed (°/min)			1.5–14.6*			
$2\theta_{max}$ (°)			70			
Range *hkl*			$-14 \le h \le 14$	$0 \le k \le 19$	$0 \le l \le 9$	
Number of independent reflections	2909	2934	2576	2860	2898	2350
Number of reflections with $I_o > 2\sigma I_o$	2238	2437	2089	2286	2317	1698
Refined parms			115			
*R*1 (%)	3.03	4.80	3.09	3.22	2.95	3.88
*wR*2 (%)	7.15	13.76	6.94	6.81	6.56	7.40
GooF	1.009	1.031	1.065	1.058	1.056	1.038

* According to reflection intensity estimated by a prescan.

TABLE 3. Fractional coordinates and displacement parameters (U_{eq} for non-hydrogen atoms, U_{iso} for hydrogen atoms) of Tutton's salts

Atom	*x*	*y*	*z*	U_{eq} (Å^2)	Metal	Atom	*x*	*y*	*z*	U_{eq} (Å^2)
M	0	0	0	0.01600(12)	Mg	OW2	–0.16687(11)	0.11337(8)	0.03085(18)	0.02245(18)
	0	0	0	0.01664(17)	Fe		–0.17268(18)	0.11702(14)	0.0311(3)	0.0265(3)
	0	0	0	0.01471(8)	Co		–0.17045(16)	0.11495(11)	0.0340(2)	0.0222(2)
	0	0	0	0.01387(7)	Ni		–0.16659(15)	0.11244(11)	0.0356(2)	0.0204(2)
	0	0	0	0.01548(7)	Cu		–0.18654(15)	0.11833(11)	0.0369(2)	0.0270(2)
	0	0	0	0.01671(11)	Zn		–0.1702(2)	0.11474(17)	0.0352(3)	0.0222(4)
K	0.13134(4)	0.34617(3)	0.34067(6)	0.03040(8)	Mg	OW3	–0.00576(12)	–0.06931(8)	0.29752(17)	0.02324(19)
	0.13292(7)	0.34612(5)	0.34165(9)	0.03318(14)	Fe		–0.0045(2)	–0.07101(15)	0.3023(3)	0.0274(3)
	0.13269(5)	0.34534(4)	0.34159(7)	0.02916(10)	Co		–0.00388(17)	–0.06892(12)	0.3000(2)	0.0226(2)
	0.13415(5)	0.34561(4)	0.34287(7)	0.02864(10)	Ni		0.00028(17)	–0.06662(11)	0.3016(2)	0.0207(2)
	0.12305(5)	0.34736(3)	0.34202(6)	0.02853(9)	Cu		–0.00266(14)	–0.06475(10)	0.28730(19)	0.0204(2)
	0.13362(8)	0.34570(5)	0.34310(10)	0.02896(15)	Zn		–0.0023(3)	–0.06799(16)	0.3000(3)	0.0225(4)
S	0.41077(3)	0.13607(2)	0.72574(5)	0.01749(7)	Mg	H11	0.208(3)	0.090(2)	0.284(4)	0.045(6)
	0.41170(5)	0.13502(4)	0.72661(8)	0.02074(13)	Fe		0.215(4)	0.088(3)	0.298(7)	0.029(8)
	0.41148(5)	0.13499(3)	0.72532(7)	0.01711(9)	Co		0.205(3)	0.091(2)	0.290(5)	0.035(7)
	0.41182(4)	0.13508(3)	0.72625(7)	0.01642(8)	Ni		0.204(3)	0.087(2)	0.292(4)	0.032(7)
	0.40127(4)	0.13607(3)	0.72269(6)	0.01757(8)	Cu		0.194(3)	0.093(2)	0.295(5)	0.055(8)
	0.41199(7)	0.13524(5)	0.72669(10)	0.01703(13)	Zn		0.199(4)	0.095(3)	0.292(6)	0.039(10)
O1	0.40448(14)	0.23014(9)	0.57271(18)	0.0333(2)	Mg	H12	0.232(2)	0.124(2)	0.104(4)	0.032(5)
	0.4065(2)	0.22972(16)	0.5758(3)	0.0370(4)	Fe		0.247(6)	0.121(5)	0.108(9)	0.061(14)
	0.40752(18)	0.23005(11)	0.5751(2)	0.0319(3)	Co		0.238(3)	0.121(2)	0.102(5)	0.048(8)
	0.40933(18)	0.22977(11)	0.5747(2)	0.0305(3)	Ni		0.223(3)	0.122(2)	0.095(5)	0.044(8)
	0.39830(16)	0.23523(10)	0.5827(2)	0.0316(3)	Cu		0.228(3)	0.122(2)	0.098(5)	0.044(7)
	0.4079(3)	0.23002(12)	0.5770(3)	0.0327(5)	Zn		0.230(4)	0.121(3)	0.105(6)	0.038(12)
O2	0.55583(12)	0.07906(11)	0.7543(2)	0.0410(3)	Mg	H21	–0.245(3)	0.104(2)	–0.054(4)	0.049(7)
	0.5553(2)	0.0764(2)	0.7503(4)	0.0441(5)	Fe		–0.262(5)	0.102(3)	–0.070(7)	0.035(9)
	0.55540(17)	0.07588(14)	0.7517(3)	0.0387(4)	Co		–0.254(4)	0.104(3)	–0.050(5)	0.058(10)
	0.55685(16)	0.07498(14)	0.7563(3)	0.0374(4)	Ni		–0.249(3)	0.102(2)	–0.051(5)	0.048(8)
	0.54389(14)	0.07577(13)	0.7409(2)	0.0359(3)	Cu		–0.265(3)	0.108(2)	–0.052(5)	0.047(8)
	0.5562(2)	0.0760(2)	0.7528(4)	0.0388(6)	Zn		–0.245(4)	0.100(3)	–0.053(6)	0.047(12)
O3	0.28666(11)	0.06067(8)	0.62018(17)	0.02365(19)	Mg	H22	–0.145(2)	0.177(2)	–0.003(4)	0.040(6)
	0.28558(18)	0.06087(14)	0.6222(3)	0.0276(3)	Fe		–0.128(6)	0.185(5)	0.034(9)	0.070(15)
	0.28472(15)	0.06080(10)	0.6189(2)	0.0232(2)	Co		–0.147(3)	0.176(2)	–0.001(5)	0.048(8)
	0.28357(14)	0.06140(10)	0.6186(2)	0.0223(2)	Ni		–0.149(3)	0.174(2)	–0.005(5)	0.042(8)
	0.27318(13)	0.06377(10)	0.61100(19)	0.0230(2)	Cu		–0.161(3)	0.184(2)	0.005(5)	0.055(8)
	0.2841(2)	0.06149(15)	0.6206(3)	0.0232(4)	Zn		–0.149(5)	0.173(3)	0.003(7)	0.057(13)
O4	0.39265(13)	0.17398(8)	0.94652(17)	0.0272(2)	Mg	H31	–0.073(4)	–0.066(2)	0.340(5)	0.075(9)
	0.3960(2)	0.17192(15)	0.9476(3)	0.0303(3)	Fe		–0.093(6)	–0.070(4)	0.341(9)	0.055(12)
	0.39463(17)	0.17267(10)	0.9464(2)	0.0260(3)	Co		–0.072(4)	–0.060(3)	0.346(6)	0.061(10)
	0.39398(16)	0.17389(11)	0.9472(2)	0.0257(3)	Ni		–0.065(4)	–0.064(3)	0.328(6)	0.075(13)
	0.38523(14)	0.16801(10)	0.94724(19)	0.0273(2)	Cu		–0.074(3)	–0.061(2)	0.325(5)	0.059(9)
	0.3954(2)	0.17307(16)	0.9477(3)	0.0255(4)	Zn		–0.084(5)	–0.063(4)	0.337(7)	0.067(16)
OW1	0.16878(12)	0.10875(9)	0.16561(19)	0.02416(19)	Mg	H32	0.027(3)	–0.131(2)	0.334(4)	0.051(7)
	0.1725(2)	0.11375(16)	0.1714(3)	0.0284(3)	Fe		0.040(6)	–0.141(5)	0.354(9)	0.061(14)
	0.17019(16)	0.11228(11)	0.1665(2)	0.0233(3)	Co		0.024(4)	–0.130(3)	0.333(5)	0.057(9)
	0.16694(15)	0.11095(11)	0.1630(2)	0.0214(2)	Ni		0.028(4)	–0.135(3)	0.328(5)	0.064(10)
	0.16072(15)	0.11203(11)	0.1636(2)	0.0261(2)	Cu		0.033(3)	–0.131(3)	0.316(5)	0.064(9)
	0.1699(2)	0.11285(16)	0.1667(3)	0.0232(4)	Zn		0.031(4)	–0.127(3)	0.329(6)	0.050(12)

that occur in distorted coordination environments. For the corresponding polyhedra, it is possible to calculate several geometrical parameters connected with the centroid of coordination (Balić-Žunić and Makovicky 1996). Eccentricity, sphericity, and volume distortion describe various geometrical aspects related to the polyhedral irregularity. These parameters are linked to the average distance from the ligands to the centroid (r_S), the standard deviation of distances from ligands to the centroid (σ_{rs}), and distance of the central atom to the centroid (Δ) by the following formulas (Balić-Žunić 2007):

linear eccentricity, $ECC = \Delta/r_S$;
linear sphericity, $SPH = 1 - \sigma_{rs}/r_S$;
volume distortion, $\nu = (V_i - V_p)/V_i$;

where V_i and V_p are ideal and observed polyhedral volume, respectively. These parameters and the volume of circumscribed sphere (V_S) were calculated using the IVTON2 software (most recent version of the IVTON program of Balić-Žunić and Vicković 1996). It should be noted that the values for the volume distortion parameters are calculated in comparison with the maximum-volume polyhedron for a given coordination number (CN): tetrahedron for CN = 4, octahedron for CN = 6, and bisdisphenoid for CN = 8.

Another polyhedral parameter, which measures the size of the distortion, is that proposed by Brown (2006):

$$\Delta R = -(0.37/N)\,\Sigma\ln(s_i/s');$$

where N is the number of bonds formed by the central atom, s_i is the valence of the ith bond and s' is the average valence of the bonds in the coordination sphere ($\Sigma s_i/N$). ΔR reflects, via bond

TABLE 5. Relevant bond distances (Å) and angles (°) of Tutton's salts

	KMgS	KFeS	KCoS	KNiS	KCuS	KZnS
S-O2	1.4630(11)	1.4647(19)	1.4628(15)	1.4668(14)	1.4676(13)	1.4643(22)
-O3	1.4734(9)	1.4783(16)	1.4780(13)	1.4768(12)	1.4825(11)	1.4802(18)
-O1	1.4779(10)	1.4830(19)	1.4794(13)	1.4787(14)	1.4771(13)	1.4749(19)
-O4	1.4802(10)	1.4787(18)	1.4814(13)	1.4838(13)	1.4799(12)	1.4811(18)
<S-O>	1.4736(10)	1.4762(18)	1.4754(13)	1.4765(13)	1.4768(12)	1.4751(19)
O1-S-O2	109.56(8)	109.58(13)	109.58(10)	109.68(10)	109.73(9)	109.66(14)
-S-O3	108.01(6)	108.06(11)	108.20(8)	108.13(8)	108.20(7)	108.08(11)
-S-O4	109.95(6)	110.13(11)	109.82(8)	109.77(8)	110.01(7)	109.69(11)
O2-S-O3	108.61(7)	108.29(11)	108.42(9)	108.65(9)	108.45(8)	108.75(12)
-S-O4	110.42(7)	110.41(12)	110.49(9)	110.39(9)	110.49(8)	110.46(12)
O3-S-O4	110.24(6)	110.31(10)	110.29(8)	110.19(8)	109.91(7)	110.16(11)
M-OW3 ×2	2.0255(10)	2.0702(17)	2.0391(13)	2.0205(13)	1.9438(11)	2.0310(19)
-OW1 ×2	2.0885(10)	2.1661(17)	2.1215(13)	2.0758(13)	2.0643(12)	2.1244(19)
-OW2 ×2	2.1012(10)	2.1708(16)	2.1369(13)	2.0850(12)	2.2752(13)	2.1337(20)
<M^{2+}-O>	2.0717(10)	2.1357(17)	2.0992(13)	2.0604(13)	2.0944(13)	2.0964(20)
OW1-M^{2+}-OW1^{I}	180	180	180	180	180	180
-M^{2+}-OW2	89.57(4)	88.85(7)	88.96(6)	88.39(5)	89.40(5)	88.62(8)
-M^{2+}-OW3	90.86(4)	90.39(7)	90.47(6)	89.55(6)	90.65(5)	89.99(8)
OW2-M^{2+}-OW2^{I}	180	180	180	180	180	180
-M^{2+}-OW3	90.54(4)	91.17(7)	90.12(5)	89.89(6)	90.87(5)	90.08(9)
OW3-M^{2+}-OW3^{I}	180	180	180	180	180	180
K-O3^{II}	2.7248(10)	2.7326(19)	2.7300(13)	2.7264(14)	2.7798(13)	2.734(2)
-O4^{III}	2.8148(11)	2.823(2)	2.8173(14)	2.8111(14)	2.8295(13)	2.8198(19)
-O1	2.8986(13)	2.916(2)	2.9015(16)	2.8859(16)	2.9075(15)	2.900(2)
-O2^{IV}	2.9398(15)	2.944(3)	2.9500(18)	2.9625(19)	2.8847(16)	2.945(3)
-O1^{IV}	2.9436(13)	2.947(2)	2.9295(16)	2.9092(16)	2.9814(14)	2.933(2)
-OW2^{V}	3.0027(10)	2.9506(17)	2.9558(13)	2.9652(14)	2.8866(14)	2.949(2)
-OW1	3.1485(11)	3.093(2)	3.0937(14)	3.1078(14)	3.1089(14)	3.093(2)
-O2^{II}	3.2961(14)	3.279(3)	3.2656(18)	3.2562(19)	3.1387(16)	3.272(3)
<K-O>	2.9711(11)	2.961(2)	2.9554(15)	2.9530(15)	2.9396(14)	2.956(2)
OW1-H11	0.76(2)	0.84(4)	0.79(3)	0.83(2)	0.83(3)	0.78(4)
-H12	0.79(2)	0.87(6)	0.82(4)	0.74(3)	0.83(3)	0.74(4)
OW2-H21	0.78(2)	0.91(4)	0.81(3)	0.81(3)	0.79(3)	0.77(3)
-H22	0.84(2)	0.92(6)	0.82(3)	0.82(3)	0.87(3)	0.77(4)
OW3-H31	0.73(3)	0.90(6)	0.75(4)	0.65(4)	0.75(3)	0.83(5)
-H32	0.83(2)	0.97(5)	0.79(3)	0.87(3)	0.87(4)	0.78(4)
O1-H32	1.85(2) 1.74*	1.68(5) 1.72*	1.86(3) 1.72*	1.79(2) 1.73*	1.80(3) 1.73*	1.88(4) 1.73*
O2-H21	1.91(2) 1.75*	1.78(4) 1.75*	1.87(3) 1.75*	1.86(3) 1.73*	1.92(3) 1.78*	1.91(3) 1.75*
O3-H11	2.04(2) 1.86*	1.97(4) 1.88*	2.00(3) 1.86*	1.97(3) 1.86*	1.93(3) 1.82*	2.02(3) 1.86*
-H31	2.02(3) 1.82*	1.82(6) 1.78*	1.99(4) 1.82*	2.08(4) 1.79*	1.93(3) 1.75*	1.89(5) 1.79*
O4-H12	2.04(2) 1.89*	1.97(6) 1.90*	2.01(3) 1.89*	2.08(3) 1.89*	1.97(3) 1.85*	2.08(4) 1.89*
-H22	1.90(2) 1.80*	1.87(6) 1.85*	1.93(3) 1.81*	1.93(3) 1.82*	1.90(3) 1.83*	1.97(4) 1.81*
H11-OW1-H12	108(2)	103(5)	110(3)	115(3)	113(2)	116(4)
H21-OW2-H22	102(2)	120(4)	104(3)	100(3)	103(3)	105(4)
H31-OW3-H32	104(3)	105(5)	106(3)	103(4)	108(3)	109(4)

Notes: Symmetry codes: ^{I} –*x*, –*y*, –*z*; ^{II} –*x* + 1/2, *y* + 1/2, –*z* + 1; ^{III} *x* – 1/2, –*y* + 1/2, *z* – 1; ^{IV} *x* – 1/2, –*y* + 1/2, *z*; ^{V} *x* + 1/2, –*y* + 1/2, *z*.
All calculations carried out with PARST (Nardelli 1983).
* Values normalized following Jeffrey and Lewis (1978) and Taylor and Kennard (1983).

TABLE 6. Bond valence sum (valence units) incident at each atom of Tutton's salts

	KMgS	KFeS	KCoS	KNiS	KCuS	KZnS
M^{2+}	2.17(1)	2.04(1)	2.01(1)	2.00(1)	2.08(1)	2.09(1)
K^{+}	0.907(4)	0.919(4)	0.930(4)	0.938(4)	0.942(4)	0.929(4)
S^{6+}	6.01(1)	5.97(2)	5.98(1)	5.97(1)	5.95(1)	5.98(2)
$O1^{2-}$	1.72 + 1HB	1.69 + 1HB	1.72 + 1HB	1.73 + 1HB	1.71 + 1HB	1.73 + 1HB
$O2^{2-}$	1.70 + 1HB	1.69 + 1HB	1.70 + 1HB	1.68 + 1HB	1.72 + 1HB	1.70 + 1HB
$O3^{2-}$	1.70 + 2HB	1.68 + 2HB	1.68 + 2HB	1.69 + 2HB	1.64 + 2HB	1.67 + 2HB
$O4^{2-}$	1.63 + 2HB	1.64 + 2HB	1.63 + 2HB	1.62 + 2HB	1.63 + 2HB	1.63 + 2HB
$OW1^{2-}$	0.41 + 2H	0.38 + 2H	0.39 + 2H	0.39 + 2H	0.42 + 2H	0.39 + 2H
$OW2^{2-}$	0.43 + 2H	0.42 + 2H	0.41 + 2H	0.42 + 2H	0.33 + 2H	0.42 + 2H
$OW3^{2-}$	0.41 + 2H	0.40 + 2H	0.39 + 2H	0.37 + 2H	0.49 + 2H	0.41 + 2H

Note: Digits in parentheses are estimated uncertainties (1σ) for cations. They were calculated according to Wang and Liebau (2007), using the standard uncertainty of bond lengths (Table 5) and the estimated standard error of bond-valence parameters (Brown and Altermatt 1985). HB = hydrogen bond (ca. 0.2 v.u.). H = O-H bond (ca. 0.8 v.u.).

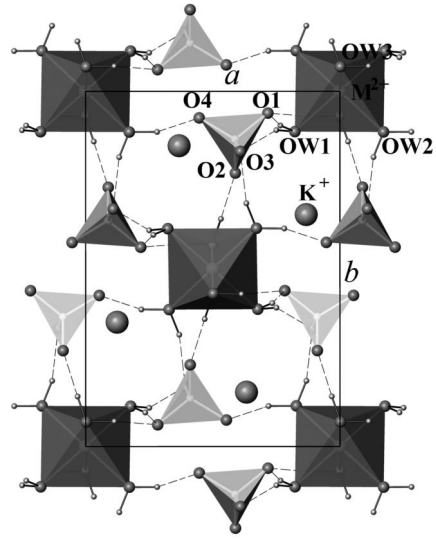

FIGURE 1. Structure of Tutton's salts as seen along [001].

valences, the deviation of the bond lengths from their average value, and it is independent from the ideal polyhedron chosen as model. Table 7 summarizes distortion indices and volumes found around the cation sites.

S in the fourfold coordination (SO_4)

The S^{6+} cation is surrounded by O1, O2, O3, and O4. The small values of ν_S and ΔR_S (ca. 0.04% and 0.0001 Å, respectively) indicate a slight distortion in the SO_4 polyhedron. The ECC_S values are also small (below 0.009), showing a slight displacement of the S^{6+} cation position from the ideal metric center of the coordination polyhedron (centroid). Such displacement is larger for KFeS and KCoS, while it is smaller for KCuS. The ECC_S shows a positive correlation with both ν_S and ΔR_S (r^2 = 0.76 and 0.96, respectively). With respect to perfect tetrahedra, the deviation of the observed bond angles from the ideal value of 109.47° is small (average deviation is about 1°). Consequently, the SO_4 group can be considered as a very slightly distorted tetrahedron.

M^{2+} in the sixfold coordination (MO_6)

The M^{2+} cation is surrounded by six ligands (OW1 × 2, OW2 × 2, OW3 × 2). Values of ν_M and ΔR_M for the MO_6 polyhedron related to Mg, Fe, Co, Ni, and Zn are quite small (ca. 0.1% and 0.002 Å), whereas they are larger for the CuO_6 polyhedron (ν_{Cu} = 0.66% and ΔR_{Cu} = 0.024 Å) because of the Jahn-Teller effect. However, the degree of this distortion appears moderate in comparison with the Jahn-Teller distortion associated with Cu^{2+} in other phases: for example, in the compound $[CuCl(C_6H_6H_4)(H_2O)][Cu(C_4H_5NO_4)Cl]\cdot H_2O$ (Gao et al. 2005), the ν_{Cu} and ΔR_{Cu} values calculated for the Cu1 and Cu2 atoms are about 6% and 0.14 Å. The centroid position coincides with the central atom M (ECC_M = 0). There is a slight deviation from sphericity for the MO_6 polyhedra centered by Mg, Fe, Co, Ni, and Zn (SPH_M about 0.98); more marked is that related to CuO_6 (SPH_{Cu} = 0.9284). The SPH_M shows a non-linear negative correlation with both ν_M and ΔR_M (r^2 = 0.99). With respect to perfect octahedra, the deviation of the observed bond angles from the ideal value of 90° is small in MO_6 (average deviation is about 1°). As a result, the ligand arrangement around the Mg, Fe, Co, Ni, and Zn atoms represent very slightly distorted octahedra. The degree of the distortion is much more significant for the Cu-centered polyhedron, in which the deviation from sphericity is the largest observed in these Tutton's salts.

TABLE 7. Polyhedral parameters: linear eccentricity (EEC), linear sphericity (SPH), volume distortion (ν), size of distortion (ΔR), volume of the circumscribed sphere (V_S), and volume of the coordination polyhedron (V_P)

	ECC	SPH	ν (%)	ΔR (Å)	V_S (Å^3)	V_P (Å^3)
			SO_4 polyhedron			
KMgS	0.0078	1	0.05	0.0001	13.41	1.642(4)
KFeS	0.0089	1	0.05	0.0001	13.49	1.652(7)
KCoS	0.0086	1	0.05	0.0001	13.45	1.647(5)
KNiS	0.0072	1	0.04	0.0001	13.49	1.651(5)
KCuS	0.0066	1	0.03	0.0000	13.49	1.652(6)
KZnS	0.0079	1	0.04	0.0001	13.45	1.647(7)
			MO_6 polyhedron			
KMgS	0	0.9825	0.06	0.002	37.25	11.85(1)
KFeS	0	0.9762	0.11	0.003	40.83	12.98(3)
KCoS	0	0.9776	0.08	0.003	38.75	12.32(2)
KNiS	0	0.9849	0.07	0.001	36.64	11.66(2)
KCuS	0	0.9284	0.66	0.024	38.49	12.17(2)
KZnS	0	0.9757	0.10	0.003	38.59	12.27(3)
			KO_8 polyhedron			
KMgS	0.0277	0.9401	7.74	0.035	109.70	43.87(4)
KFeS	0.0255	0.9452	7.67	0.030	108.36	43.37(8)
KCoS	0.0240	0.9454	7.66	0.029	107.88	43.18(5)
KNiS	0.0239	0.9445	7.66	0.030	107.62	43.07(5)
KCuS	0.0275	0.9594	7.06	0.018	106.62	42.95(5)
KZnS	0.0257	0.9453	7.60	0.029	107.84	43.20(7)

Note: Parameters calculated using IVTON2, except for ΔR.

K in the eightfold coordination (KO_8)

The K^+ cation is surrounded by O1, $O1^{IV}$, $O2^{II}$, $O2^{IV}$, $O3^{II}$, $O4^{III}$, OW1, and $OW2^{V}$. In general, the volume distortion ν_K for KO_8 has moderate values (average values of 7.57%), the largest and the smallest ν_K value being observed in the KMgS (7.74%) and KCuS (7.06%) phases, respectively. A similar trend is observed for ΔR_K (average values of 0.029 Å). The centroid position in KO_8 shows displacement from central atom in all compositions. Such displacement is larger for KMgS (ECC_K = 0.0277), while it is smaller for KNiS (ECC_K = 0.0239). The deviation from sphericity for the KO_8 polyhedron is moderate (SPH_K is about 0.95). SPH_K shows a negative correlation with both ν_K and ΔR_K (r^2 > 0.97). Because KO_8 is the only polyhedron that shows both deviation of the central atom from the centroid position (ECC_K) and deviation of the ligands from sphericity (SPH_K), and ν_K and ΔR_K have appreciable values, it can be considered as the polyhedron with the highest distortion indices observed in these Tutton's salts. Exception from this trend is given by the KCuS phase, which shows ΔR_K and SPH_K smaller than the corresponding ΔR_M and SPH_M (Table 7). The smallest distortion indices (SPH_K, ν_K, and ΔR_K) related to KCuS, suggest an increase in regularity of the KO_8 polyhedron linked to the Jahn-Teller distortion around the Cu^{2+} cation. In general, in the $K_2[M(H_2O)](SO_4)_2$ Tutton's salts, the degree of polyhedral distortion increases with increasing coordination number.

For the corresponding octacoordinate polyhedron, several regular polyhedra can be chosen as models (Alvarez et al. 2005). To understand which is the best ideal shape to describe the KO_8 polyhedron, the V_S/V_i ratio characteristic of each ideal octacoordinate polyhedron was examined (Makovicky and Balić-Žunić 1998; Balić-Žunić 2007): 2.3070 (bisdisphenoid), 2.3906 (square antiprism with maximum volume), 2.4184 (hexagonal bipyramid), 2.4369 (Archimedean square antiprism), 2.4891 (bicapped trigonal prism), and 2.7204 (cube). Comparing the ideal V_S/V_i ratios of these polyhedra with the observed V_S/V_P ratios of KO_8, it is immediately apparent (Fig. 2) that the best fit is to the bicapped trigonal prism.

Crystal chemistry

In the SO_4 polyhedron, the small values of distortion indices (ECC_S, ν_S, and ΔR_S) reflect the strong S-O bond valences of about 1.5 valence unit, which support a rigid geometrical configuration. ECC_S is positively correlated with both M-OW1 and M-OW2 bond lengths (r^2 > 0.82). The mean <S-O> bond length is statistically identical in all samples (Table 5), showing that it is not affected by changes in cation occupancies at the adjacent octahedral site. Differences in the S-O bond lengths result predominately from hydrogen bonds at O1, O2, O3, and O4. In

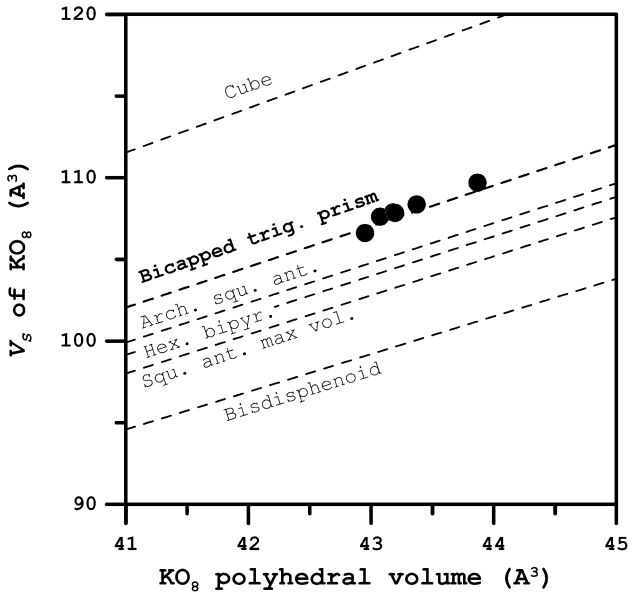

FIGURE 2. KO_8 observed volume (V_P) vs. volume of circumscribed sphere (V_S) plot. The dashed lines represent the various types of V_S/V_i ratios for ideal octacoordinate polyhedra. Symbol dimensions are proportional to 2σ.

particular, in the SO_4 group O2 accepts a single hydrogen bond and is only weakly bonded to two K atoms. Both O1 and O2 are acceptors of a single hydrogen bond, whereas O3 and O4 accept two hydrogen bonds. As a result hydrogen bond distances for O1 and O2 are smaller than those for O3 and O4 (Table 5).

In the MO_6 polyhedron, individual *M*-O bond lengths follow a general *M*-OW2 ≅ *M*-OW1 > *M*-OW3 sequence. The mean bond length (<*M*-O>) is generally smaller than the intermediate *M*-OW1 bond length. The exception is observed for the Jahn-Teller active cation Cu^{2+}, where <*M*-O> is greater than *M*-OW1. The higher deviation of Cu^{2+}-O bond lengths from their average value causes an expansion (ΔR_{Cu} ca. 0.02 Å) in CuO_6 with respect to other octahedra. The effect of this expansion compensates for the smaller ionic radius of Cu^{2+} with respect to Zn^{2+} (Shannon 1976), leading to very similar octahedral mean bond lengths: <Cu^{2+}-O> = 2.094 and <Zn^{2+}-O> = 2.096 Å. This explains the very similar unit-cell volume observed for KCuS and KZnS: 658.2 and 658.3 $Å^3$, respectively.

In general, <*M*-O> for these Tutton's salts varies linearly with the ionic radii (Shannon 1976) of the *M* cation, <IR_M>, according the following regression formula (r^2 = 0.95):

$$<M\text{-O}> = 0.8597 \cdot <IR_M> + 1.4619.$$

The positive correlation between ΔR_M and <IR_M> for M^{2+} = Mg, Fe, Co, Ni, Zn (r^2 = 0.78), and the negative one between SPH_M and <IR_M> (r^2 = 0.76), show that the steric effect yields only small deviations from the octahedral regularity. In contrast, more significant is the contribution to the irregularity of the CuO_6 polyhedron ascribed to electronic effects (i.e., electronic anisotropies of Cu^{2+}).

The bond valence analysis indicates a positive difference between the bond valence sum at the Mg site and the formal valence of the Mg atom (about 0.2 valence unit). According to the bond-valence theory (e.g., Brown 2002), this difference, site valence mismatch, leads to a considerable overbonding of the Mg atom (about 8%). Conversely, there is an underbonding of K atoms in all samples (Table 6): the most evident is that in the KMgS phase (about 10%).

In the KO_8 polyhedron, the mean <K-O> bond length and the observed volume are not constant for all the studied phases, but they vary from 2.940 to 2.971 Å and from 11.66 to 12.98 $Å^3$, respectively. This suggests an expansion of the bond environment around K due to interaction with the second-nearest neighbors. The KO_8 volume (and of course <K-O>) shows a strong negative correlation with bond valence sum at the K site (Fig. 3). Consequently, any change in the KO_8 size is accompanied by a change in the bond valence sum at K. This relationship reflects the "softness" of the K^+ cation, i.e., the ability of its electronic ground state to distort in response to the surroundings. The bond valence sum at K is correlated with the *M*-OW1 bond length of Fe, Co, Ni, Zn, and Cu (Fig. 4). Consequently, both the bond valence and size in KO_8 change as a function of *M*-OW1, except for the KMgS phase which falls off the regression line of Figure 4. This anomalous behavior of the Mg atom reflects both the most overbonded state at the Mg site and the most underbonded state at the K site. In the latter both the K-OW1 and K-OW2 bond lengths (3.00 and 3.15 Å, respectively) are larger than corresponding bonds in the other studied phases (ca. 2.95 and 3.10 Å, respectively). It is worth noting that a contraction of K-OW1 and K-OW2 bond lengths, and conversely the lengthening of Mg-OW1 and Mg-OW2, should result in a reduction of both under and overbonding at the K and Mg sites, respectively. However, if such a reduction in the site-valence mismatch at the K and Mg sites occurs, it would be counterbalanced by a further weakening of OW1-H12···O4 and OW1-H11···O3 bonds that are the longest of the hydrogen bonds network (Table 5). This would eventually result in a destabilization of the structure. With regard to the

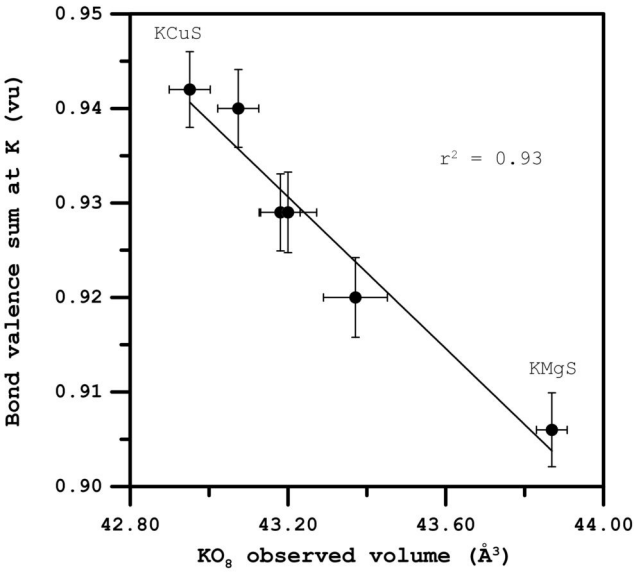

FIGURE 3. With a decrease in bond valence sum at the K site, KO_8 observed volume increases. v.u. = valence unit. Error bars are proportional to σ.

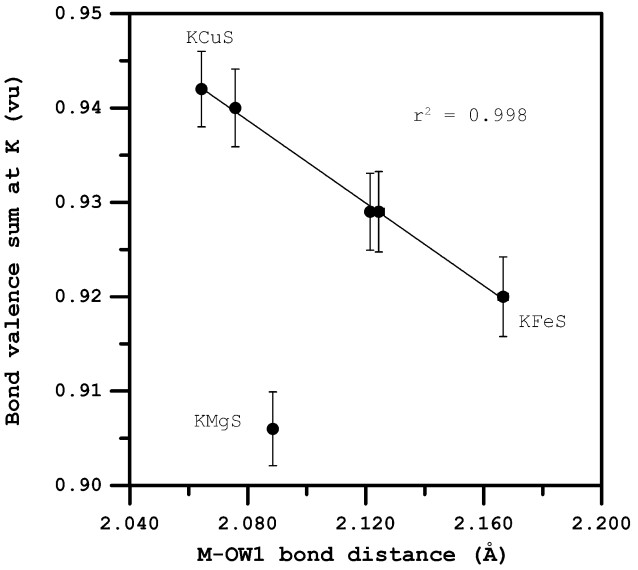

FIGURE 4. The relationship between bond valence sum at the K site and *M*-OW1 bond length shows the overall influence of the MO_6 polyhedron on the K-O bond valences and, therefore, on the KO_8 size. Symbol dimensions and error bars, where shown, are proportional to σ.

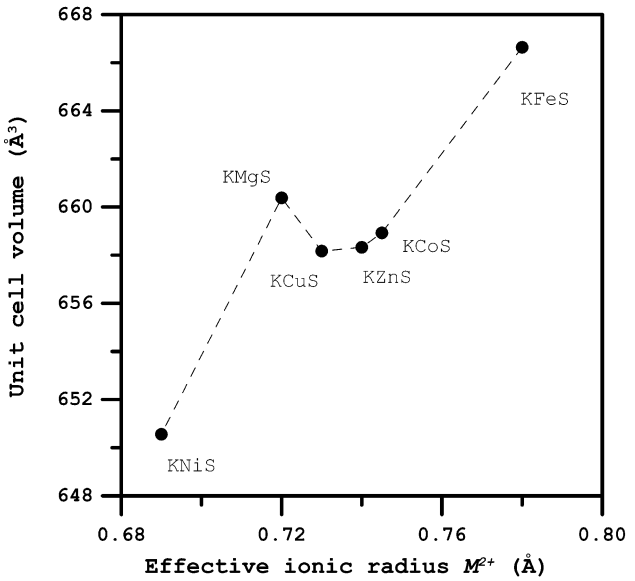

FIGURE 5. Variation of the unit-cell volume with the ionic radii of M^{2+} (Shannon 1976), showing the marked deviation of Mg-phase from the expected trend. Symbol dimensions are proportional to 2σ.

distortion parameters, ΔR_K (and likewise ν_K and SPH_K) shows correlations with K-O3 and K-OW2 bond lengths ($r^2 > 0.90$), with *M*-OW2 bond valence ($r^2 = 0.93$). ECC_K shows correlation with the bond valence sum at the *M* site ($r^2 = 0.78$). In general, geometrical changes associated with the KO_8 polyhedron are mainly linked to interactions with the MO_6 polyhedron and seem to be dictated by bond-valence requirements, which result, in turn, from changes in *M*-O individual lengths and from changes in the distribution of the bond strengths over the oxygen atoms coordinated to K.

The overall effect of the interaction among the SO_4, MO_6, and K^+ is insignificant in terms of polyhedral distortion for SO_4 and MO_6, but is much more significant in terms of influence on degree of the distortion and size for KO_8. The large univalent cation K^+ is "soft" and the K-O lengths show a lengthening over a considerable range in response to interaction with M^{2+} cations.

Unit-cell modification

Cell parameters (*a*, *b*, and *c*) of $K_2[M^{2+}(H_2O)_6](SO_4)_2$ show only weak positive correlations with $\langle IR_M \rangle$ ($r^2 < 0.67$), mainly because of KMgS and KCuS deviations. The *b* cell parameter shows a strong correlation ($r^2 > 0.90$) with both bond valence sum at K and KO_8 volume (negative and positive trend, respectively). In these correlations, however, KMgS deviates as a consequence of the relationship between *M*-OW1 and bond valence sum at K (Fig. 4). The β angle shows a negative correlation with both *M*-OW2 bond length ($r^2 = 0.86$) and $\langle IR_M \rangle$ ($r^2 = 0.95$), with the omission of KCuS in the latter.

The unit-cell volume increases with increasing $\langle IR_M \rangle$. This trend is well followed by Fe-, Co-, Zn-, and Ni-phases, whereas the Cu-phase and, especially, the Mg-phase deviate from it (Fig. 5). If the former deviation is ascribable to the rather distorted environment around Cu^{2+}, the latter appears strongly inconsistent with the Mg size. In fact, given the ionic radius for Mg^{2+} (Shannon 1976), the unit-cell volume of KMgS should be smaller than that related to cations with larger ionic radii, such as Zn^{2+} and Co^{2+}. In contrast, the unit-cell volume of KMgS exceeds those of KZnS and KCoS (+2.05 and +1.45 Å^3, respectively). To explain this inconsistency, structural changes outside the first octahedral coordination sphere of *M* were explored. Without regard to the H atoms, the second coordination sphere of *M* comprises 12 oxygen atoms (O1 × 4, O2 × 2, O3 × 4, O4 × 2), and ^{12}M-O distances ranging from 3.94 to 4.25 Å. For this MO_{12} polyhedron, geometrical parameters were calculated using the IVTON2 program (Table 8). The MO_{12} volume values reflect the expansion of the second coordination sphere of the Mg atom with respect to those of Zn and Co, and this explains the larger value of its unit-cell volume (Fig. 6). The size of this expansion can be measured by the difference between the volume of the circumscribed sphere of MO_{12} and that of MO_6 (ΔV_{SM}, Table 8). For all phases, ΔV_{SM} increases with increasing KO_8 volume ($r^2 = 0.80$), indicating that the observed non-constant values of the KO_8 size change in accordance with expansion of the second coordination sphere of the *M*. In fact, the Mg-phase has the largest values of the KO_8 volume and ΔV_{SMg}, while the Cu-phase has

TABLE 8. Geometrical parameters related to the MO_{12} polyhedron representing the second coordination sphere of *M*

	$^{12}SPH_M$	$^{12}\nu_M$ (%)	$^{12}V_P$ (Å^3)	$^{12}V_{SM}$ (Å^3)	ΔV_{SM} (Å^3)
KMgS	0.9792	13.35	152.3(1)	290.21	252.96
KFeS	0.9775	13.35	153.7(2)	292.87	252.04
KCoS	0.9787	13.32	151.5(1)	288.62	249.87
KNiS	0.9772	13.12	149.1(1)	283.46	246.82
KCuS	0.9800	13.02	149.9(1)	284.70	246.22
KZnS	0.9774	13.23	151.1(2)	287.64	249.05

Notes: Parameters calculated using IVTON2; ECC = 0; ΔV_{SM} = difference between the volume of sphere fitted to the position of O1 (×4), O2 (×2), O3 (×4), O4 (×2), and that to positions OW1 (×2), OW2 (×2), OW3 (×2). Note that the O1, O2, O3, and O4 anions represent the second coordination sphere of MO_{12}, while the OW1, OW2, and OW3 anions represent the first coordination sphere of MO_6.

the smallest KO_8 volume and an anomalously low ΔV_{SCu} (Tables 7 and 8). According to the negative correlation between the bond length and bond valence (e.g., Brese and O'Keeffe 1991; Brown 2002), increase in K-O bond length leads to decrease in K-O bond valence. Figure 7 illustrates the negative correlation between ΔV_{SM} and bond valence sum at the K site, which explains the most underbonded state observed at the K site for KMgS and the highest for KCuS.

As the octahedral distortion around Cu (which increases the CuO_6 size, bringing it closer to that of ZnO_6 and causes deviations from the expected structural trends) can be related to the Jahn-Teller effect, the higher ionicity of the Mg atom could be the cause for its anomalous behavior observed in Tutton's salts. A similar anomalous stereochemical behavior of the Mg atom was also observed in kieserite- and blödite-type compounds (Hawthorne et al. 1987; Wildner and Giester 1991; Giester and Wildner 1992; Stoilova and Wildner 2004), and it was attributed to different bonding character of the Mg-O bond compared to the 3*d* transition cations. As was explained with the aid of infrared spectroscopy in the blödite-type compounds (Stoilova and Wildner 2004), it appears that in Tutton's salts the deviation of Mg from the structural trend of the transition-metal cations and the relative expansion of the Mg second coordination sphere seem to be consistent with the weakening of the hydrogen bonds in the structure connected to differences in the bonding character of Mg and transition metals when coordinated by water molecules.

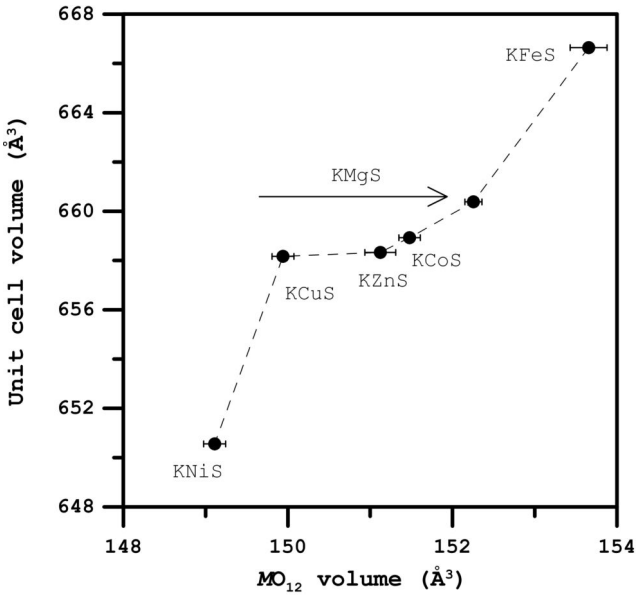

FIGURE 6. Variation of the unit-cell volume with the MO_{12} volume, showing the alignment of the Mg-phase along the expected trend. The horizontal arrow shows the displacement of KMgS with respect to Figure 5. Symbol dimensions and error bars, where shown, are proportional to σ.

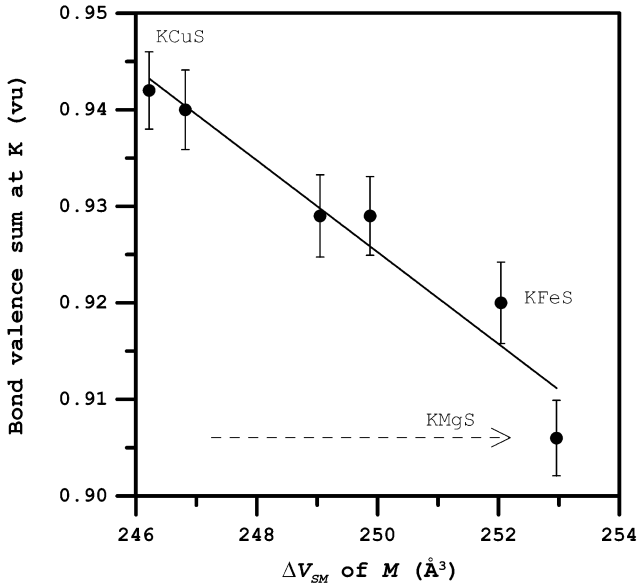

FIGURE 7. Variation of the bond valence sum at K with the ΔV_{SM}, showing the alignment of the Mg-phase closer to the expected trend. The horizontal dashed arrow line shows the displacement of KMgS with respect to Figure 4. Error bars are proportional to σ.

ACKNOWLEDGMENTS

This work received financial support from Università di Roma "La Sapienza." The authors thank L.A. Groat (University of British Columbia) and T. Balić-Žunić (University of Copenhagen) for their careful and helpful reviews.

REFERENCES CITED

Agnew, M. (1998) The formation of hardpans within tailings as possible inhibitors of acid mine drainage, contaminant release and dusting. Ph.D. thesis, University of Adelaide, Australia.

Alvarez, S., Alemany, P., Casanova, D., Cirera, J., Llunell, M., and Avnir, D. (2005) Shape maps and polyhedral interconversion paths in transition metal chemistry. Coordination Chemistry Reviews, 249, 1693–1708.

Balić-Žunić, T. (2007) Use of three-dimensional parameters in the analysis of crystal structures under compression. In A. Grzechnik, Ed., Pressure-Induced Phase Transitions, p. 157–184. Transworld Research Network, Trivandrum, Kerela, India.

Balić-Žunić, T. and Makovicky, E. (1996) Determination of the Centroid or "the Best Centre" of a Coordination Polyhedron. Acta Crystallographica, B52, 78–81.

Balić-Žunić, T. and Vickovic, I. (1996) IVTON—Program for the calculation of geometrical aspects of crystal structures and some crystal chemical applications. Journal of Applied Crystallography, 29, 305–306.

Ballirano, P. and Belardi, G. (2006) Rietveld refinement of Tutton's salt $K_2[Fe(H_2O)_6](SO_4)_2$. Acta Crystallographica, E62, i58–i60.

Brese, N.E. and O'Keeffe, M.O. (1991) Bond-valence parameters for solids. Acta Crystallographica, B47, 192–197.

Brown, I.D. (2002) The Chemical Bond in Inorganic Chemistry: The Bond Valence Model, 288 p. International Union of Crystallography Monographs on Crystallography No. 12, Oxford University Press, U.K.

——— (2006) On measuring the size of distortions in coordination polyhedra. Acta Crystallographica, B62, 692–694.

Brown, I.D. and Altermatt, D. (1985) Bond-valence parameters obtained from a systematic analysis of the Inorganic Crystal Structure Database. Acta Crystallographica, B41, 244–247.

Cotton, F.A., Daniels, L.M., Murillo, C.A., and Quesada, J.F. (1993) Hexaaqua dipositive ions of the first transitions series: New and accurate structures; expected and unexpected trends. Inorganic Chemistry, 32, 4861–4867.

Dhandapani, M., Thyagu, L., Arun Prakash, P., Amirthaganesan, G., Kandhaswamy, M.A., and Srinivasan, V. (2006) Synthesis and characterization of potassium magnesium sulfate hexahydrate crystals. Crystal Research and Technology, 41, 328–331.

Euler, H., Barbier, B., Klumpp, S., and Kirfel, A. (2000) Crystal structure of Tutton's salts, $Rb_2[M^{II}(H_2O)_6](SO_4)_2$, M^{II} = Mg, Mn, Fe, Co, Ni, Zn. Zeitschrift für Kristallographie, New Crystal Structures, 215, 473–476.

Euler, H., Barbier, B., Meents, A., and Kirfel, A. (2003) Crystal structure of Tutton's salts, $Cs_2[M^{II}(H_2O)_6](SO_4)_2$, M^{II} = Mg, Mn, Fe, Co, Ni, Zn. Zeitschrift für Kristallographie, New Crystal Structures, 218, 409–413.

Gao, X.-L., Wei, Y.-B., Li, Y.-P., and Yang, P. (2005) Aqua(2,2′-bi-1*H*-imidazole) chloro-copper(II) chloro(iminodiacetato)-copper(II) monohydrate. Acta Crystallographica, C62, m10–m12.

Garavelli, C.L. (1964) Mohrite, a new mineral in the boriferous Tuscan area. In Atti Accademia Nazionale Lincei, Rendicondi, Classe di Scienze Fisiche, Matematiche e Naturali, 36, 524–533 (in Italian).

Giester, G. and Wildner, M. (1992) The crystal structure of kieserite-type com-

pounds. II. Crystal structure of *Me*(II)$SeO_4 \cdot H_2O$ (*Me* = Mn, Fe, Co, Ni, Zn). Neues Jahrbuch für Mineralogie Monatschefte, 3, 135–144.

Hawthorne, F.C., Groat, L.A., Raudsepp, M., and Ercit, T.S. (1987) Kieserite, $Mg(SO_4)(H_2O)$, a titanite group mineral. Neues Jahrbuch für Mineralogie Abhandlungen, 157, 121–132.

Jeffrey, G.A. and Lewis, L. (1978) Cooperative aspects of hydrogen bonding in carbohydrates. Carbohydrate Research, 60, 179–182.

Kannan, K.K. and Viswamitra, M.A. (1965) Crystal structure of magnesium potassium sulfate hexahydrate $MgK_2(SO_4)_2 \cdot 6H_2O$. Zeitschrift für Kristallographie, 122, 161–174.

King, P.L., Lescinsky, D.T., and Nesbitt, H.W. (2004) The composition and evolution of primordial solutions on Mars, with application to other planetary bodies. Geochimica et Cosmochimica Acta, 68, 4993–5008.

Larsen, E.S. and Shannon, E.V. (1920) Boussingaultite from South Mountain, near Santa Paula, California. American Mineralogist, 5, 127–128.

Makovicky, E. and Balić-Žunić, T. (1998) New measure of distortion for coordination polyhedra. Acta Crystallographica, B54, 766–773.

Nardelli, M. (1983) PARST computer program. Computational Chemistry, 7, 95–98.

North, A.C.T., Phillips, D.C., and Mathews, F.S. (1968) A semi-empirical method of absorption correction. Acta Crystallographica, A24, 351–359.

Shannon, R.D. (1976) Revised effective ionic radii and systematic studies of interatomic distances in halides and chalcogenides. Acta Crystallographica, A32, 751–767.

Sheldrick, G.M. (1997) SHELXL 97-1. Program for crystal structure determination. University of Göttingen, Germany.

Simmons, C.J., Stratemeier, H., Hitchman, M.A., and Riley, M.J. (2006) Influence of lattice interactions on the Jahn-Teller distortion of the $[Cu(H_2O)_6]^{2+}$ ion: Dependence of the crystal structure of $K_2[Cu(H_2O)_6](SO_4)_{(2x)}(SeO_4)_{(2-2x)}$ upon the sulfate/selenate ratio. Inorganic Chemistry, 45, 1021–1031.

Spencer, R.J. (2000) Sulfate minerals in evaporate deposits. In C.N. Alpers, J.L. Jambor, and D.K. Nordstrom, Eds., Sulfate Minerals, 40, p. 173–192. Reviews in Mineralogy and Geochemistry, Mineralogical Society of America, Chantilly, Virginia.

Stoilova, D. and Wildner, M. (2004) Blödite-type compounds $Na_2Me(SO_4)_2 \cdot 4H_2O$ (*Me* = Mg, Co, Ni, Zn): Crystal structures and hydrogen bonding systems. Journal of Molecular Structure, 706, 57–63.

Taylor, R. and Kennard, O. (1983) Comparison of X-ray and neutron diffraction results for the N-H···O = C hydrogen bond. Acta Crystallographica, B39, 133–138.

Thomsen, K., Rasmussen, P., and Gani, R. (1996) Correlation and prediction of thermal properties and phase behavior for a class of aqueous electrolyte systems. Chemical Engineering Science, 51, 3675–3683.

Wang, X. and Liebau, F. (2007) Influence of polyhedron distortions on calculated bond-valence sums for cations with one lone electron pair. Acta Crystallographica, B63, 216–228.

Wildner, M. and Giester, G. (1991) The crystal structure of kieserite-type compounds. I. Crystal structure of *Me*(II)$SO_4 \cdot H_2O$ (*Me* = Mn, Fe, Co, Ni, Zn). Neues Jahrbuch für Mineralogie Monatschefte, 7, 296–306.

Wilson, A.J.C. (1995) International Tables for Crystallography, vol. C, Table 6.1.1.4, p. 500–502. Kluwer Academic Publishers, Dordrecht.

Yakhontova, L.K., Siderenko, G.A., Stolyarova, T.I., Plyusnina, I.I., and Ivanova, T.L. (1976) Nickel-containing sulfates from the oxidation zone of the Norilskiye deposits. Zapiski Vsesoyuznogo Mineralogicheskogo Obshchestva, 105, 710–720 (in Russian).

Zoltov, M.Y. and Shock, E.L. (2001) A hydrothermal origin for the sulfate-rich ocean of Europa. Abstract to Lunar and Planetary Science XXXII, 1990.

Manuscript received December 17, 2007
Manuscript accepted July 15, 2008
Manuscript handled by Barry Bickmore